

# Fundamentals of Developer-Resist Interactions for Line-Edge Roughness and Critical Dimension control in Model 248 nm and 157 nm Photoresists\*

Vivek M. Prabhu<sup>§</sup>, Michael X. Wang, Erin L. Jablonski, Bryan D. Vogt, Eric K. Lin, Wen-li Wu, Polymers Division, National Institute of Standards and Technology, Gaithersburg, MD 20899-8541

Darío L. Goldfarb, Marie Angelopoulos,  
IBM T. J. Watson Research Center, Yorktown Heights, NY 10598

Hiroshi Ito,  
IBM Almaden Research Center, San Jose, CA 95120

## 1. ABSTRACT

Organic polar solvent (1-butanol) versus aqueous base (tetramethylammonium hydroxide, (TMAH)) development quality are distinguished by neutral versus charged polymer (polyelectrolyte) dissolution behavior of photoresist bilayers on silicon substrates comprising poly(4-hydroxystyrene) and poly(4-*tert*-butoxycarbonyloxystyrene), PHOST and PBOCSt, respectively. This model line-edge was broadened by photoacid catalyzed deprotection to a final interfacial width of 35.7 Å and subjected to different developers. 1-butanol develops with an increased penetration depth than aqueous base development consistent with an increased solubility of the protected containing component in the organic solvent. This enhanced dissolution with the polar solvent results in an increased surface roughness of 73 Å, whereas the development with TMAH at concentrations between (0.1 to 1.1) M<sup>1</sup> leads to surface roughness between (4.5 to 14.4) Å, as measured by atomic force microscopy. These measurements suggest that the elimination of resist swelling, in the presence of a protection gradient, is a viable strategy to reduce roughness and control critical dimensions. The influence of added salt to developer solutions was also examined by developing the model bilayer. A decrease in surface roughness from (10 to 6.5) Å was observed between (0 to 0.70) M KCl in 0.26 M TMAH.

Keywords: developer, dissolution, LER, CD, polyelectrolyte, reflectivity, AFM, roughness, swelling

## 2. INTRODUCTION

To quantify the developer influence on photoresist critical dimension (CD) control and line-edge roughness (LER) minimization, a scheme is necessary to address material versus optical contributions. A model photoresist bilayer geometry was constructed to simplify this problem using standard processing conditions and a blanket ultra-violet (UV) light exposure. This method leads to a well defined deprotection gradient that can be tuned by post-exposure bake processing<sup>2,3</sup>, hence emphasizing the material contribution. This reaction front gradient is used to understand developer strength, additives, swelling and reaction front width effects on the final CD and model LER.

Recently, polyelectrolyte effects were demonstrated to be the source of photoresist solubility, a direct result of the acid-base equilibrium.<sup>4,5</sup> These polyelectrolyte effects have also been correlated to wafer performance<sup>6</sup>. This result is extended to examine neutral versus polyelectrolyte dissolution effects on CD and LER with 1-butanol versus TMAH

---

\* Official contribution of the National Institute of Standards and Technology; not subject to copyright in the United States

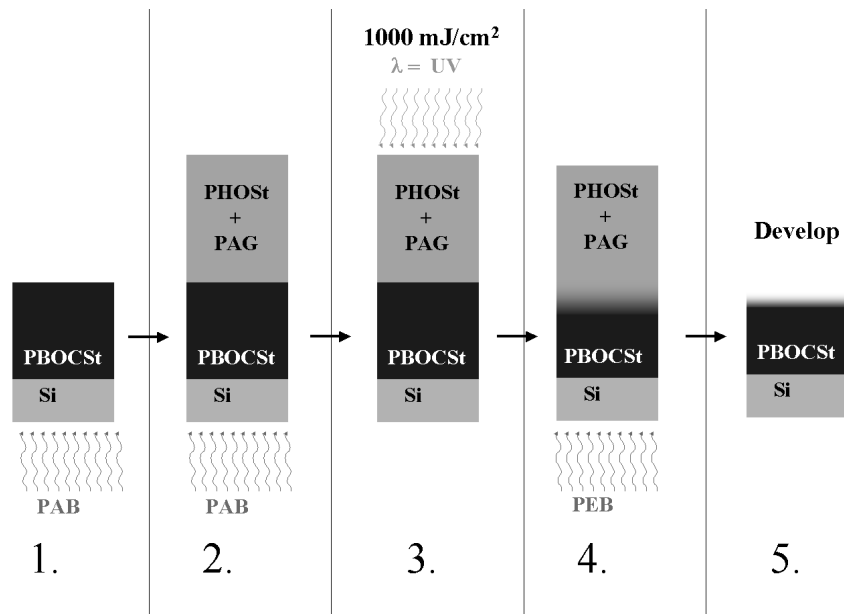
<sup>§</sup> Corresponding author, vprabhu@nist.gov, Tel.: (301) 975-3657; fax (301) 975-3928.

development. The dissolution with 1-butanol leads to expected swelling and recovery upon drying, which results in high surface roughness.

### 3. EXPERIMENTAL

#### 3.1. Preparation of Bilayers

Bilayer structures for the developer studies were prepared on semiconductor-grade silicon wafers (approximately 1 mm thick and 150 mm diameter) as follows: 5 min exposure to oxygen plasma, followed by removal of the native oxide layer by subsequent immersion into a solution of  $(10 \pm 2)$  % volume fraction HF and  $(5 \pm 2)$  % volume fraction  $\text{NH}_4\text{F}$  in ultra pure water for  $(15 \pm 5)$  s. An oxide layer was regrown in a UV/Ozone chamber for  $(120 \pm 1)$  s followed by priming with hexamethyldisilazane (HMDS) vapor. The lower layer consisting of the deuterio poly(4-*tert*-butoxycarbonyloxystyrene) ( $d_{12}$ -PBOCSt) ( $M_{r,n} = 21000$ ,  $M_{r,w}/M_{r,n} = 2.1$ ) was spin-coated from a propylene glycol methyl ether acetate (PGMEA) solution and post-apply baked (PAB) for 60 s at 130 °C. The corresponding deprotected polymer, poly(4-hydroxystyrene) (PHOSt) ( $M_{r,n} = 5260$ ,  $M_{r,w}/M_{r,n} = 1.12$ ), was spin-coated from a 1-butanol solution directly onto the lower layer. The PHOSt layer is loaded with 5 % mass fraction of the photoacid generator, di(*tert*-butylphenyl) iodonium perfluorooctanesulfonate (PFOS). The bilayer is subjected to another PAB for 60 s at 130 °C. The model bilayer stack was exposed with a broadband UV dose of 1000  $\text{mJ}/\text{cm}^2$  to generate acid within the top PHOSt layer followed by post-exposure bake (PEB) at 100 °C for 30 s. The use of deuterated PBOCSt allows for the measurement of the *t*-BOC deprotection profile using neutron reflectivity. Bilayer samples were then developed by immersion into tetramethylammonium hydroxide (TMAH) aqueous base solutions for 30 s followed by immersion for 30 s into fresh deionized water with resistivity 18.0  $\text{M}\Omega\text{-cm}$  purified by a Milli-Q UF Plus system.<sup>7</sup> TMAH solutions were prepared by dilution of a stock solution (mass fraction of 10 %), purchased from Aldrich Chemicals, using deionized water. A summary of the processing scheme is shown below.



Scheme 1. Photoresist bilayer processing scheme using PBOCSt and PHOSt acid feeder layer

The latent image, after the PEB, was measured on 5 control wafers prepared identically. Neutron reflectivity was performed on all control wafers, prior to development; these wafers were identical within the resolution of the instrument indicating cross-wafer comparisons can be made with confidence. The subsequent specular reflectivity measurements are performed on samples developed with (0.1 to 1.1) M TMAH concentrations or 1-butanol. In most

cases, the wafers were cleaved into two pieces such that multiple development protocols could be performed on the same spun-cast wafer.

The model bilayer stack for developer studies with added KCl were prepared with the same wafer treatment as described earlier, however, protonated PBOCSt was used. The PEB temperature was 100 °C for 30 s or 90 s. Bilayer samples were then developed by immersion into 0.26 M TMAH solutions containing varying levels of added KCl from (0.1 to 1.1) M for 30 s followed by immersion for 30 s into fresh deionized water with resistivity 18.0 M $\Omega$ -cm purified by a Milli-Q UF Plus system. Analytical grade KCl was used to prepare solutions with varying KCl concentrations.

The developed and dried films were characterized by atomic force microscopy (AFM) to measure the root-mean square (RMS) roughness, which provides a comparison to the reflectivity modeled interfacial width. The tapping-mode surface image of all samples was measured using a Digital Dimension 3100 and corrected with a plane-fit. The reported RMS roughness was calculated using the Digital software.

### 3.2. Neutron and X-ray Reflectivity

Specular reflectivity provides a high resolution measurement of thin films with angstrom resolution in thickness and interfacial width. The specular reflection from thin films is observed as a series of Kiessig fringes, related to the film thickness, which are then damped due to finite interfacial width. These interfaces are typically modeled as a step interface convoluted with a Gaussian function, leading to error function profiles.<sup>8</sup> Since the origin of the reflection is due to the gradient in the scattering length density profile, the deuterium protecting group ( $d_{12}$ -t-BOC) scheme was used to provide neutron reflectivity contrast between the PBOCSt/PHOST bilayer.<sup>2</sup> Thus for a single bilayer sample, the neutron reflectivity measurement provides the high resolution deuterium protection profile complementing the electron density profile measured by x-ray reflectivity. The bilayer was measured after a PEB that provides the reaction-diffusion interfacial broadening due to thermal-induced diffusion of the photoacid.

Neutron reflectivity (NR) measurements were performed on the NG 7 reflectometer at the NIST Center for Neutron Research. The absolute reflected intensities were measured at the specular condition as a function of angle ( $\theta$ ), defining the scattering wave vector normal to the film,  $Q = 4 \pi \lambda^{-1} \sin \theta$ , where  $\lambda$  is the fixed incident neutron wavelength of 4.75 Å with resolution  $\Delta\lambda/\lambda = 0.025$ . X-ray reflectivity (XR) measurements were performed on a modified x-ray reflectometer with Cu- $k_{\alpha}$  radiation with filtered wavelength of 1.54 Å with resolution  $\Delta\lambda/\lambda = 6 \times 10^{-5}$ .

The elastic coherent scattering length per volume ( $Q_c^2 = 16 \pi \rho_v$ ) profiles in Å<sup>-2</sup>, versus distance ( $Z$ ) from the silicon substrate are determined from the model fits to the XR and NR reflectivity data.  $\rho_v$  is the scattering length density, an intensive property defined by the ratio of coherent monomer scattering length to specific volume. The scattering length density profiles are converted to mass density fraction and t-BOC protection fraction from knowledge of the component scattering length density values for XR and NR, respectively.

The uncertainties are calculated as the estimated standard deviation of the mean. In the case where the limits are smaller than the plotted symbols, the limits are left out for clarity. Fits of the reflectivity data are made by a weighted least-squares regression algorithm.

### 3.3. Small-Angle Neutron Scattering

Small-angle neutron scattering (SANS) was performed on the NG1 guide 8 m instrument at the National Center for Neutron Research (NCNR), National Institute of Standards Technology. A 7-position sample changer was used to examine the small-angle scattering by dilute polymer and pure solvent solutions in which the scattering contrast was achieved by using partially deuterated poly(4-hydroxystyrene) ( $d_3$ -PHOST) in light water (H<sub>2</sub>O) containing various levels of basic and salt components. The  $d_3$ -PHOST used for the small-angle neutron scattering experiments, was custom synthesized by Polymer Source, Inc., Dorval, Quebec<sup>6</sup> with weight-average relative molecular weight of  $M_{r,n} = 8,750 \text{ g mol}^{-1}$  and polydispersity  $M_{r,w}/M_{r,n} = 1.07$ . This solid glassy powder was dissolved directly in aqueous

base solutions with and without added salts to a nominal concentration of  $0.04 \text{ g cm}^{-3}$ . Additional details regarding sample preparation and method can be found elsewhere.<sup>4</sup>

## 4. RESULTS AND DISCUSSIONS

### 4.1. Neutral versus polyelectrolyte solution behavior

The solubility switch of chemically amplified photoresists is due to the ionization of a well defined fraction of weakly acidic sites in the presence of aqueous base solution as shown in Fig. 1(a). This ionization leads to long-ranged electrostatic repulsive interactions between polymer segments, which can be measured as a correlation peak by small-angle neutron scattering (SANS). The main results are shown in Fig. 1(b) for a PHOSt sample dissolved in 0.26 M TMAH solution at a polymer concentration of  $0.04 \text{ g cm}^{-3}$ . Similar results are observed for 157 nm poly(norbornene hexafluoroisopropanol) (PNBHFA)<sup>6</sup>. When the origin of solubility is due to the short-ranged interactions, no peak is observed as demonstrated by polymers dissolved in casting solvents, such as PGMEA and 1-butanol at equal concentrations. The development of photoresists must pass from the case of an unionized polymer to a polyelectrolyte through the copolymer composition design.

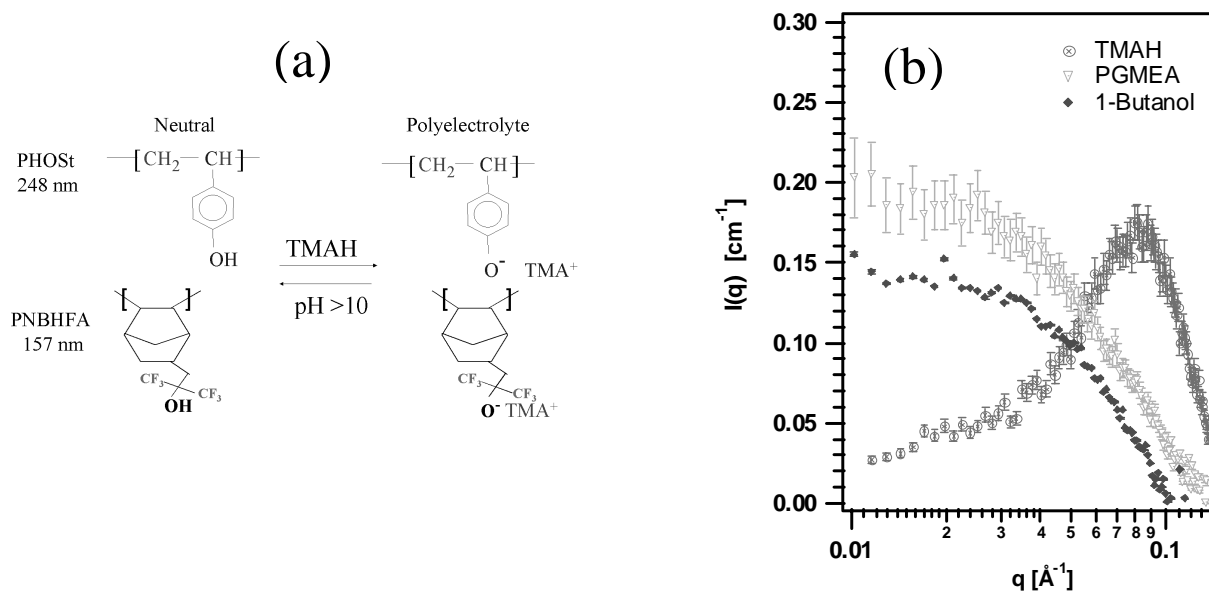


Figure 1. (a) Chemical equilibrium for PHOSt and PNBHFA. (b) Small-angle neutron scattering results for  $d_3$ -PHOSt in 0.26 M TMAH solution, PGMEA, and 1-butanol. Polyelectrolyte effects are only present in the aqueous base.

### 4.2. Aqueous base versus 1-butanol Development

The solvent quality difference between an aqueous base versus polar solvent appears through neutral versus polyelectrolyte effects as shown in Fig. 1. The neutral polymer dissolution by a good solvent, without ionization, leads to a distinct solvent swollen penetration front, or steady state gel-like layer<sup>9-11</sup>. The gel layer thickness is influenced by the solvent quality and molecular weight. This contrasts current work with model 248 nm photoresists thin films in which the polyelectrolyte dissolution by aqueous base does not lead to the formation of a gel layer, but dissolution occurs via a reaction etch-like mechanism that does not require a thick solvent swelled front<sup>12</sup>. In order to test the swelling versus non-swelling development, the model reaction front interface was developed by 0.10 M TMAH and 1-

butanol. The critical dimension is determined by the total film thickness as measured by x-ray reflectivity and the model LER quantified by AFM. Additional information is provided by the *t*-BOC protection profile as measured by neutron reflectivity. Only the main results after fitting the reflectivity data to obtain the scattering length density profile are presented in these proceedings. In Fig. 2, the *t*-BOC protection volume fraction (solid line), as determined by neutron reflectivity, and mass fraction (dotted line) determined by x-ray reflectivity are shown as a function of distance (*Z*) from the silicon substrate.

The 0.10 M TMAH developed sample is shown in Fig 2 (a). The mass density profile (dotted line) appears sharp with top surface interfacial roughness determined by XR of 16 Å. While the *t*-BOC protection profile shows a compositional change as a result of development. The final deprotection interfacial surface roughness is low, 26 Å. However, the broad compositional profile is a result of developing a portion of the reaction front interfacial width. The majority of the compositional broadening is a result from the initial 35.7 Å diffuse reaction front width<sup>2</sup>. The AFM determined surface RMS roughness is 4 Å. The AFM roughness is a different measure of surface roughness than the reflectivity methods. The emphasis of the AFM technique is only the height fluctuations that are accessible by the AFM tip. The reflectivity methods, due to the short wavelength, provide an improved quantification of the solid-air interface<sup>8</sup>.

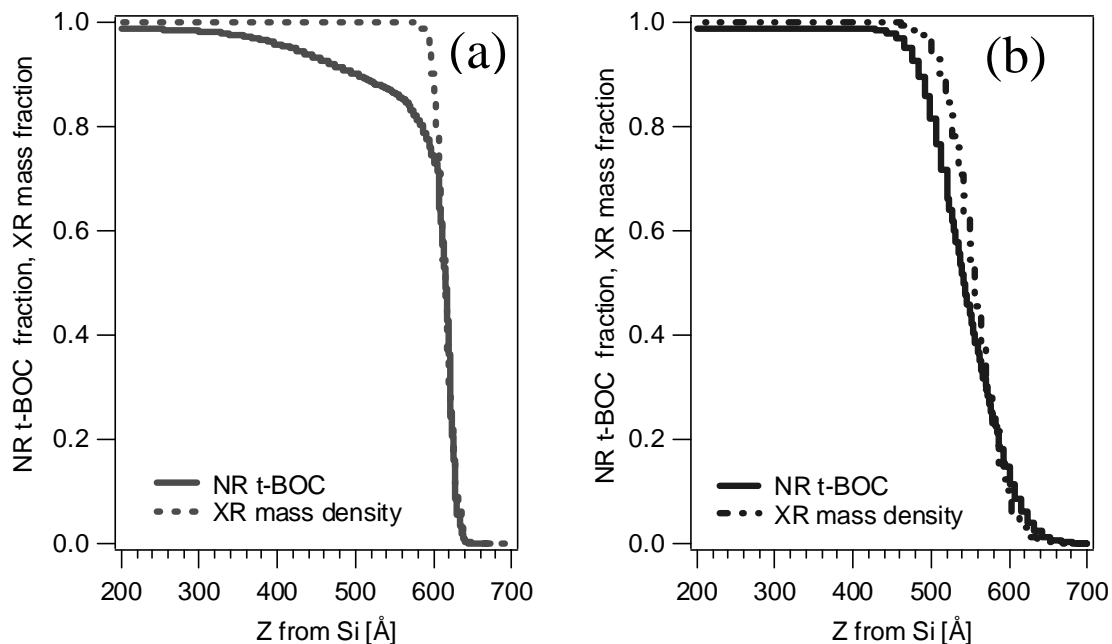


Figure 2. X-ray and neutron reflectivity determined mass fraction and *t*-BOC protection profiles, respectively. (a) 0.10 M TMAH developed results and (b) Butanol developed results.

The butanol developed sample, Fig 2 (b), however, has a mass density (dotted line) polymer–air surface roughness of 70 Å as compared to the aqueous base developed sample, 16 Å. Butanol development induces surface structural changes as seen by the broad mass density and compositional profile. The mass density profile follows the *t*-BOC compositional profile due to the broad solubility switch when using the polar solvent, except that for a given distance *Z* the mass density is higher than the *t*-BOC profile. This is expected because a significant fraction of PHOS<sub>t</sub> remains undeveloped, as confirmed by near-edge x-ray absorption fine structure (NEXAFS) spectroscopy. The development by 1-butanol suggests that a higher protection fraction is permitted for dissolution, when compared to aqueous base development. The true phase diagram as a function of copolymer composition, determined by thermal deprotection, for butanol development is in progress.

Comparing the final critical dimensions, 0.10 M TMAH development led to a developed film thickness of 597 Å whereas with butanol the CD was 531 Å. This 66 Å deeper penetration illustrates the phase diagram difference between the two respective solvents. The butanol was able to penetrate and dissolve deeper within the reaction front leading to

the CD difference. However, in the process the enhanced surface roughness may have resulted from the penetration and collapse of the swelled dissolution front. The butanol development depth estimates the solubility switch to be 89 % protection, however NEXAFS data quantify the surface to be 30 % PBOCSt functionality at the top 20 Å and 50 % PBOCSt functionality at a depth of 50 Å. This discrepancy with the neutron reflectivity data suggests that the dissolution process leads to a surface rearrangement upon drying. Hence, the fundamentals of surface swelling and recovery should prove to be an important issue for next generation resists at the 193 nm and 157 nm nodes. The CD appears to be a function of the solvent type, suggesting that mixing polar and aqueous base solvent may be a viable method of tuning the solubility switch as well as CD and LER.

The swelling at the dissolution front, consistent with *case II* kinetics, has been the subject of recent studies for neutral polymer dissolution completed as a function of molecular weight and solvent quality by mixtures of good and poor solvents. Although interferometer methods do not measure a gel layer; the dissolution kinetics follow the *case II* form<sup>13,14</sup>. This form is consistent with a solvent penetration front as in the neutral polymer system,<sup>11</sup> however the photoresist problem is further complicated by the presence of the compositional gradient. During the final stages of dissolution the previously good solvent encounters the high degree of protection leading to a poor solvent quality. This results in a switch in dissolution behavior with a partitioning of solvent mixtures at the interfacial front. This partitioning of aqueous base and water remains to be measured within a photoresist, but is predicted using a Poisson-Boltzmann model for electrolyte distribution from a uniformly charged interface.<sup>15-17</sup>

### 4.3. Aqueous base strength

The development with aqueous base is a dynamic process as the final film thickness and interfacial widths are a function of TMAH concentration. One concentration was presented in Fig. 2, however, several concentrations spanning from 0.10 M to 1.1 M TMAH were completed. The effect of increased TMAH concentration leads to an enhanced development depth (CD variation) and increased surface roughness. The ability to penetrate further into the film, shown in Fig. 3 (a), suggests that the solubility-switch is a function of the TMAH concentration. The solubility-switch is often quantified with dose-to-clear experiments after development with a standard 0.26 M TMAH solution. These bilayer experiments show that higher *t*-BOC concentrations dissolve in higher TMAH as observed by the deeper development depth. This also results in a broader compositional profile, shown in Fig. 3 (b) from a plot of interfacial widths as measured by neutron and x-ray reflectivity,  $\sigma_{NR}$  and  $\sigma_{XR}$ , respectively and the AFM RMS roughness,  $\sigma_{AFM}$ .

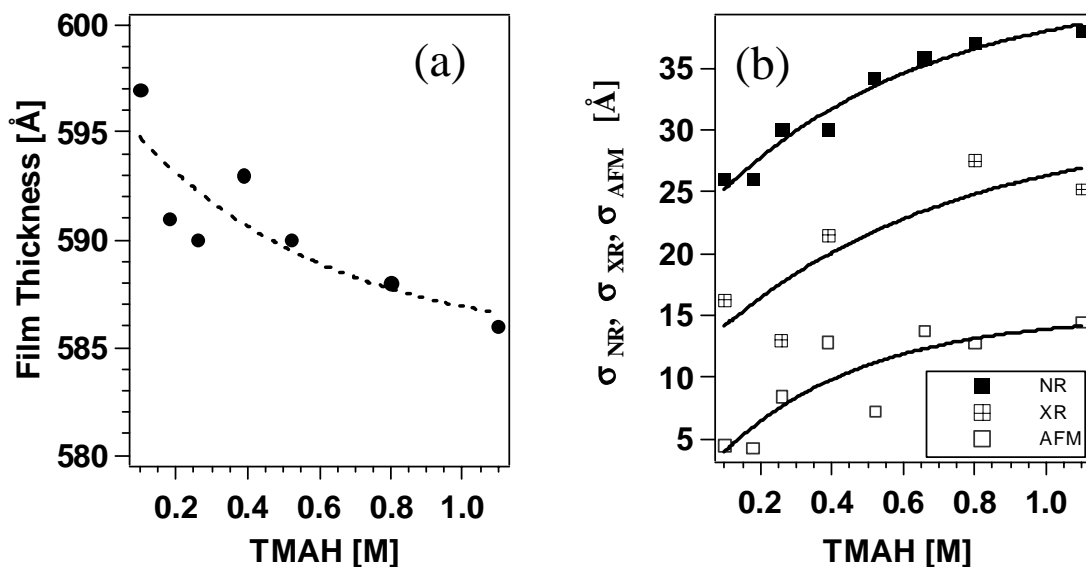


Figure 3. Critical dimension variation as a function of TMAH base developer concentration. Influence of developer on the surface roughness as measured by AFM, x-ray and neutron reflectivity. Lines are guides.

In addition to the developer-induced broadened compositional profile the AFM results (solid circles) show a systematic increase in surface roughness from (4.5 to 14.4) Å with increased TMAH concentration between (0.1 to 1.1) M. This roughness is smaller than that of the butanol developed sample,  $\sigma_{AFM} = 74$  Å. This demonstrates the model line-edge topology is a function of developer concentration. This dependence is coupled with the presence of the composition gradient, a feature in true lithographic line-edges generated by aerial-image contrast and photoacid generator diffusion.<sup>18</sup> These results confirm the modeled interfacial width increase by reflectivity and suggest that the compositional roughness includes a contribution from surface roughness (height). However, we cannot explain quantitatively the degree of compositional versus height roughness in the NR measurements.

The solubility switch can be designed with base developer concentration in addition to changing resist chemistry. The ability to penetrate deeper into the PBOCSt with higher base concentration is a result; however it can not be ascertained without supporting light scattering or osmotic pressure experiments if the solvent quality increases for higher *t*-BOC protection with increased TMAH concentration. The increased TMAH penetration of order 10 Å could lead to the propagation of the surface layer of order of the chain dimensions. If this is the origin, then the surface layer will be molecular weight dependent. This is observed for neutral polymer dissolution as the gel-layer thickness increases with molecular weight. Thus the molecular dimensions remain a design parameter in the dissolution of photoresists as molecular weight dependent roughness was observed in earlier single-layer resist studies<sup>19</sup>.

The neutron reflectivity data imply compositional heterogeneity after development and restructuring at the polymer-air interface.<sup>2</sup> This restructuring will be enhanced by increased mobility due to water and base penetration, as observed in PHOSt films<sup>20,21</sup>. Without the NR experiments, the TMAH developer-effect could only be inferred from AFM surface roughness and would only indicate the height-origin roughness, along with the lateral correlation, not surface restructuring of a minor chemical component.

#### 4.4. Bilayer-Development : Added salt influence

The model bilayer geometry was also used to quantify the role of added salt in the development of the controlled *t*-BOC protection gradient. For the present case, the interfacial *t*-BOC composition widths are (40 and 100) Å for (30 and 90) s PEB, respectively, estimated by neutron reflectivity. We present the main results of the AFM roughness in Fig. 4 as a function of development by 0.26 M TMAH with varying concentration of added KCl salt.

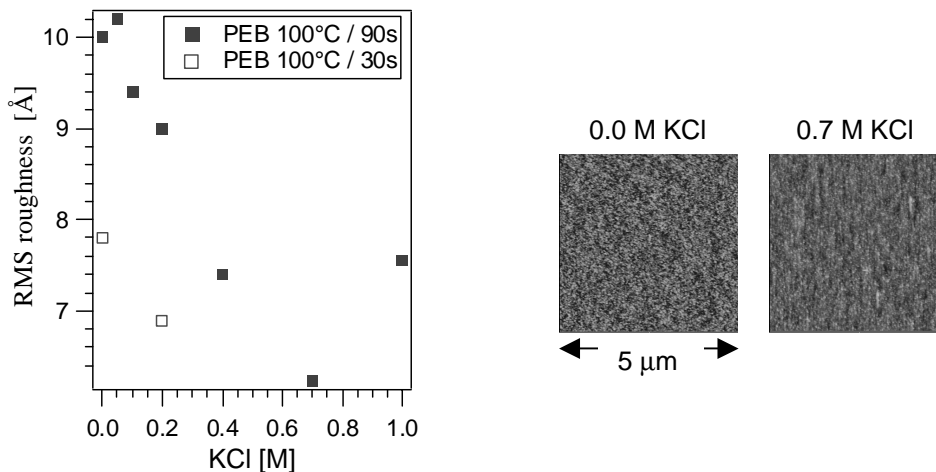


Figure 4. Left, AFM analysis of surface roughness versus KCl salt concentration for development with 0.26 N TMAH. Right, representative AFM images for development with 0.0 M and 0.7 M KCl, corresponding to post-exposure bake at 100 °C for 90 s.

After development, the AFM images were analyzed for the RMS roughness. Development with a 0.26 M TMAH solution led to a surface RMS roughness of 10 Å. As the added KCl concentration increased from (0.05 to 0.70) M, a persistent decrease in roughness from (10 to 6.5) Å was observed. An apparent increase in the roughness was observed with the 1.0 M KCl sample. The mechanism for the improvement is not clear because the kinetics of dissolution will

also influence the roughness. However, the reduction of the surface roughness by the presence of the added salt correlates well with screening of the polyelectrolyte effects. With the increased ionic strength the coil dimensions are reduced, due to screening, and elimination of the correlation peak. The persistence of the large scale aggregation with added salt may be related to the expected poor solvent conditions at the highest KCl concentration<sup>6</sup>. The developed film thickness of  $(540 \pm 10)$  Å was measured using interferometry and showed no change with added KCl. This indicates the depth of development, or CD variation, is not a function of the ionic strength, but primarily by the ionizing effect of aqueous base.

## 5. CONCLUSIONS

A model reaction front bilayer was used to quantify the influence of polar versus aqueous base development, developer strength, and salt additives to developer solutions to probe the materials contribution to CD control and LER minimization. 1-butanol develops with an increased penetration depth compared to aqueous base development indicating an increased solubility of the protected containing component. This enhanced dissolution with the polar solvent results in an increased RMS surface roughness of 73 Å, whereas the development with TMAH concentrations between (0.1 to 1.1) M leads to surface roughness between (4.5 to 14.4) Å, as measured by atomic force microscopy. These measurements suggest that eliminating swelling, expected for 1-butanol development, is a viable strategy to reduce roughness and control critical dimensions. The influence of added salt to developer solutions showed a decrease in surface roughness from (10 to 6.5) Å when the salt concentration was varied from (0 to 0.70) M KCl in 0.26 M TMAH. The role of salt appears to influence the surface features and not influence the CD, as the total film thickness remained unchanged.

## 6. ACKNOWLEDGMENTS

This work was supported by the Defense Advanced Research Projects Agency under grant N66001-00-C-8083 and the NIST Office of Microelectronics Programs. This work utilized facilities supported in part by the National Science Foundation under Agreement No. DMR-9986442. Two of the authors (ELJ & BDV) acknowledge support from the National Research Council-National Institute of Standards and Technology Postdoctoral Fellowship Program.

## REFERENCE LIST

1. The accepted SI unit of concentration, mol/L has been represented by the symbol M in order to conform to the conventions of this journal.
2. Lin, E.K., Soles, C.L., Goldfarb, D.L., Trinque, B.C., Burns, S.D., Jones, R.L., Lenhart, J.L., Angelopoulos, M., Willson, C.G., Satija, S.K., and Wu, W.L., *Science* **297**(5580), 372 (2002).
3. Houle, F.A., Hinsberg, W.D., Morrison, M., Sanchez, M.I., Wallraff, G., Larson, C., and Hoffnagle, J., *Journal of Vacuum Science & Technology B* **18**(4), 1874 (2000).
4. Prabhu, V.M., Jones, R.L., Lin, E.K., and Wu, W.L., *Journal of Vacuum Science and Technology B* **21**, 1403 (2003).
5. Prabhu, V.M., Jones, R.L., Lin, E.K., Soles, C.L., Wu, W.L., Goldfarb, D.L., and Angelopoulos, M., *Proceedings of the SPIE, Advances in Resist Technology and Processing XX* **5039**, 404 (2003).
6. Prabhu, V.M., Wang, M., Jablonski, E., Soles, C.L., Vogt, B., Jones, R.L., Lin, E.K., Wu, W.L., Goldfarb, D.L., Angelopoulos, M., and Ito, H., *Proceedings of the 13th International Conference on Photopolymers, RETEC 2003 in press*, (2003).
7. Certain commercial equipment and materials are identified in this article in order to specify adequately the experimental procedure. In no case does such identification imply recommendation by the National Institute of Standards and Technology, nor does it imply that the material or equipment identified is necessarily the best available for this purpose.

8. Russell, T., *Materials Science Reports* **5**, 171 (1990).
9. Ribar, T., Bhargava, R., and Koenig, J.L., *Macromolecules* **33**, 8842 (2000).
10. Ribar, T., Koenig, J.L., and Bhargava, R., *Macromolecules* **34**, 8340 (2001).
11. Ueberreiter, K., *The Solution Process*, (Academic Press, 1968) Chap. 7, pp.220-257.
12. Houle, F.A., Hinsberg, W.D., and Sanchez, M.I., *Macromolecules* **35**(22), 8591 (2002).
13. Burns SD, Schmid GM, Trinque, B.C., Willson, J., Wunderlich, J., Tsiartas PC, Taylor, J., Burns, R., and Willson CG, *Proceedings of the SPIE* **5039**, 1063 (2003).
14. Hinsberg, W.D., Lee, S., Ito, H., Horne, D., and Kanazawa, K., *Proceedings of the SPIE* **4345**, 1 (2001).
15. PMV Resibois, *electrolyte theory; an elementary introduction to a microscopic approach*, (Harper & Row, New York, 1968).
16. J. N. Israelachvili, *intermolecular and surface forces*, 2nd ed. (Academic Press, San Diego, CA, 1992).
17. Schmid GM, Burns SD, Tsiartas PC, and Willson CG, *Journal of Vacuum Science and Technology B* **20**(6), 2913 (2002).
18. Reynolds, G. and Taylor, J., *Journal of Vacuum Science and Technology B* **17**, 334 (1999).
19. Cutler, C., Mackevich, J., Li, J., O'Connell, D., and Brainard, R., *Proceedings of the SPIE, Advances in Resist Technology and Processing XX* **5037**, (2003).
20. Soles, C.L., Jones, R.L., Lenhart, J.L., Prabhu, V.M., Wu, W.L., Lin, E.K., Goldfarb, D.L., and Angelopoulos, M., *Proceedings of the SPIE* **5039**, 366 (2003).
21. Berger, C. and Henderson, C.L., *Polymer* **44**(7), 2101 (2003).